GSA DATA REPOSITORY 2014185

Experimental evidence for fluvial bedrock incision by suspended and bedload sediment

Joel S. Scheingross [1*], Fanny Brun[1,2], Daniel Y. Lo[1], Khadijah Omerdin[1], and Michael P. Lamb[1]

1. SCALING FOAM-TO-ROCK EROSION

The erosion rate of natural rock and concrete has been show to depend primarily on the substrate tensile strength, σ_T (Sklar and Dietrich, 2001). To test this scaling relationship for polyurethane foam, we designed a set of abrasion mill experiments eroding foam of different tensile strength ($0.3 < \sigma_T < 17$ MPa, Table DR2) and density (0.06 to 0.96 g/cm^3) while holding all other variables constant, including sediment load (150 g) and grain size (D = 6 mm). These experiments are identical to erosion-rate versus tensile-strength experiments presented in Sklar and Dietrich (2001), except here we use a foam substrate rather than rock or concrete. Results show foam erosion rates by mass loss, E_m, varied inversely with tensile strength from ~10^1 to 10^{-2} g/hr, and were slightly lower than E_m measurements from Sklar and Dietrich (2001) for material of similar tensile strength (Fig. DR1A). Accounting for the low density of foam compared to rock results in a reasonable match between foam and rock erosion, where volumetric erosion rates, E_v, scale with σ_T^{-2} (Fig. DR1B). This agreement suggests that foam acts as a suitable rock analog.

Note that Sklar and Dietrich (2004) further proposed that erosion rate depends on material Young's Modulus, Y, and a (material specific) non-dimension constant, k_v. Unlike natural rock which has little variation in Y and k_v, the Young's Modulus of foam used in this study varied from 3.9 to 330 MPa. This implies that to achieve the observed relationship between foam tensile strength and erosion rate, either k_v must vary in proportion to Y (which goes against the theoretical expectation of constant k_v (Engle, 1978)), or that Young's Modulus may have little influence on erosion rate, as has recently been suggested (Beyeler et al., 2009). In either case, the agreement in erosion-rate versus tensile-strength relationship for foam, natural rock, and concrete allows results obtained between the three substrates to be directly compared.

2. SEDIMENT CONCENTRATION MEASUREMENTS

We sampled suspended and bedload sediment within abrasion mills using 6.4 mm diameter siphons inserted through the abrasion mill walls, a sampling velocity (~0.65 ± 0.1 m/s) similar to the mean flow velocity (Winterstein and Stefan, 1983), and sample volumes that did not exceed 1.75 L (~12% of the abrasion mill water volume). Sediment concentration was measured by weighing and drying the samples, and weighing the sediment.

3. SECONDARY CIRCULATION

We used high speed video (240 frames per second) looking up through the bottom of a clear abrasion mill with foam removed to track particle motion and quantify secondary flow circulation. We manually tracked individual particle trajectories for distances of 1 – 4 full rotations about the mill, and averaged trajectories over 7 frames to calculate the ratio of

azimuthal to radial distance traveled. For five grains of 6.8 mm diameter, we found median values of azimuthal to radial distance traveled ranged from ~7 – 17. Particle trajectories for grains smaller than 6 mm could not be measured due to high particle velocities and small particle size which exceeded the speed and resolution of our high speed camera.

Sklar and Dietrich (2001; 2004) attributed suspension-regime erosion in abrasion mill experiments to secondary circulation, which they argued induced bedload transport in a way not representative of natural rivers. However, our observations are consistent with previous workers who showed that high concentrations of particles and active particle-bed interactions are expected near the bed (i.e., in a bedload layer) even within the suspension regime (e.g., Rouse, 1937; McLean, 1992). Furthermore, although secondary circulation is an important component of flow in the abrasion mills, several observations suggest it did not dominate particle trajectories or strongly influence bedrock erosion rates. First, secondary circulation in natural rivers with flow around bends as well as in straight channels is of similar magnitude (~10% of the mean azimuthal flow velocity (Dietrich and Smith, 1983; Nikora and Roy, 2012)) to our abrasion mill observations (Fig. DR2; Movies DR1–4). Second, the agreement between sediment-concentration measurements and Rouse-profile predictions (Fig. 2) suggest the abrasion mills reasonably replicate natural river fluid flow and sediment transport. Third, we observed fluting and grooves on the eroded foam surfaces parallel to the azimuthal flow direction, suggesting radial sediment transport due to secondary circulation did not exert a detectable influence on erosion.

4. ROLE OF SLOPE, FLOW DEPTH, SEDIMENT SIZE, AND SEDIMENT LOAD

Suspension of sediment during fluvial transport can be achieved either by decreasing particle size (i.e., lowering settling velocity, w_s), or increasing fluid shear stress (i.e., increasing shear velocity, u_*). In the experiments presented here, we decreased grain size while holding shear velocity and sediment load constant to achieve suspension. While tractable experimentally, this is not an ideal representation of natural bedrock rivers where the transition from bedload to suspension regime transport occurs primarily due to increases in shear velocity associated with flood events, which additionally tend to increase sediment supply (e.g., Leopold et al., 1964). Here we explore how changes in grain size, shear velocity, and sediment supply influence erosion rates in both the bedload and suspension regimes.

We ran the total-load and saltation-abrasion models under variable transport stage, τ_*/τ_{*c}, where τ_* is the non-dimensional Shields stress defined as

$$\tau_* = \frac{\tau}{\left(\rho_s - \rho_f\right) gD} \ , \qquad \text{(DR1)}$$

τ is bed shear stress, g is acceleration due to gravity, ρ_s = 2650 kg/m^3 and ρ_f = 1000 kg/m^3 are the sediment and fluid densities, respectively, and τ_{*c} = 0.03 is the critical Shields stress for sediment motion. We assumed steady, uniform flow such that

$$\tau = \rho_f u_*^2 = \rho_f ghS \ , \qquad \text{(DR2)}$$

where h and S are the channel flow depth and slope, respectively. Under these assumptions, increases in τ_*/τ_{*c} arise from increasing h or S, or decreasing D. The total-load model is dependent upon h and S individually, whereas the saltation-abrasion model is dependent upon

shear velocity (i.e., the product hS). We varied transport stage to cover conditions from incipient motion to well within the suspension regime ($10^0 < \tau_*/\tau_{*c} < 10^4$). Values of τ_*/τ_{*c} do not correspond to identical values of u_*/w_s across different model runs; however, the transition from bedload to suspension regime transport generally occurs when τ_*/τ_{*c} exceeds ~20-40. We ran two separate scenarios, first for a constant sediment load, q_s, and second, letting $q_s = 0.5q_{sc}$, where $q_{sc} = 5.7(RgD^3)^{1/2}(\tau_* - \tau_{*c})^{3/2}$ is the sediment transport capacity calculated using the empirical fit of Fernandez Lueque and van Beek (1976), and $R = (\rho_s - \rho_f)/\rho_f$ is the submerged specific density of sediment. For all cases we used base conditions representative of the South Fork Eel River, California, USA (D = 60 mm, h = 0.95 m, S = 0.0053, q_s = 8.9 x 10^{-4} m^2/s), which has been used as a reference site for the saltation-abrasion and total-load models previously (Sklar and Dietrich, 2004; 2006; 2008; Lamb et al., 2008). Models were run by varying one of either grain size, channel slope, or flow depth while holding the remaining two variables constant.

Under constant sediment load, parameterizations of the total-load and saltation-abrasion models generally agree within the bed load regime ($\tau_*/\tau_{*c} < \sim 20$), but diverge within the suspension-regime (Fig. DR3A). The saltation-abrasion model predicts that erosion rates tend towards zero as the threshold for suspension is approached regardless of how changes in transport capacity are achieved (thin gray lines in Fig. DR3A), in contrast to total-load model predictions (black lines in Fig. DR3A). When transport stage varies with grain size (as was the case for the abrasion mill experiments presented here), the total-load model predicts erosion rates decrease with increasing τ_*/τ_{*c} due to reduced kinetic energy of fine grain impacts, asymptotically approaching zero erosion near the threshold for viscous dampening (dashed black line in Fig. DR3). For transport stage varying with flow depth (black dashed-dotted line), or varying with slope (solid black line), both of which are likely in field situations but which we were unable to test experimentally, the total-load model predicts non-zero erosion rates. Increases in transport stage reduce near-bed sediment concentration due to faster particle advection and the lofting of a portion of the sediment load above the bedload layer as particles enter suspension. These effects decrease the number of particle impacts, and in turn, erosion rates. For the case of varying slope, decreases in near-bed sediment concentration are offset by increases in impact velocity for $\tau_*/\tau_{*c} > \sim 100$, such that suspension-regime erosion rates match and can exceed bed load-regime erosion rates (see Lamb et al. (2008) for further discussion).

Bedrock erosion in mountain channels occurs during floods large enough to mobilize bed-sediment, and increases in flood-magnitude generally yield increases in sediment supply (e.g., Leopold et al., 1964). Repeating the above analysis for sediment supply proportional to transport capacity (Fig. DR3B) gives markedly different total-load model predictions than under constant sediment supply (Fig. DR3A), as setting $q_s = 0.5q_{sc}$ maximizes erosion rates for a given grain size and shear velocity (Sklar and Dietrich, 2004). When transport stage is varied by reducing grain size, erosion rates decrease with transport stage well before the threshold for suspension in the saltation-abrasion model is reached (thin gray dashed line in Fig. DR3B), because increased sediment supply does not offset the effect of reduced kinetic energy of impact for fine grains. When transport stage is varied by changing shear velocity, total-load erosion rates increase monotonically with τ_*/τ_{*c} (solid and dashed-dotted black lines in Fig. DR3B), and suspension-regime erosion rates can exceed bedload regime erosion rates by multiple orders of magnitude. Thus, for large-magnitude floods in bedrock rivers, we expect suspension-regime

erosion to contribute significantly to, and in cases dominate, the total fluvial abrasion signal, as likely occurred during typhoon-induced storms in the Da'an River, Taiwan (Cook et al, 2012). Additionally, in the suspension regime, bedrock erosion can occur even if the sediment supply exceeds the bedload transport capacity, because the excess sediment, which otherwise would form a static cover and protect the bed, can be transported as suspended load.

Saltation-abrasion and total-load erosion rate predictions can also be compared to those predicted using a stream power model (e.g., Howard and Kerby, 1983),

$$E = K\tau^{\gamma} \qquad \text{(DR3)}$$

where we set K = 0.41 mm / (year Pa) and γ = 1 to match the observed long-term erosion rates in the South Fork Eel River (Sklar and Dietrich, 2006). Unlike the saltation-abrasion and total-load models, stream power predicts monotonically increasing erosion rate with transport stage, independent of sediment supply, slope, flow depth, or grain size (thick gray dashed line in Fig. DR3). When sediment supply is proportional to sediment transport capacity, the ratio of suspension-regime to bedload-regime erosion rates predicted by the total-load model roughly matches that predicted by stream-power for $2 < \tau_*/\tau_{*c} < \sim 200$ (Fig. DR3B).

5. DA'AN RIVER SUSPENSION CALCULATIONS

We calculated u_*/w_s in the Da'an River, Taiwan for all reaches in which Cook et al. (2012) report data (their Table III) for a characteristic typhoon-induced flood discharge of 1300 m^3/s. We solved for shear velocity by combining Equations DR1 and DR2 using reported values of non-dimesnional Shields stress and the medium grain diameter (D = 15 cm) (Cook et al., 2012). We estimated terminal settling velocity for a range of particle sizes using the Dietrich (1982) empirical formula with values appropriate for natural particles (Corey Shape Factor = 0.8; Powers Roundness = 3.5), and defined the maximum grain size expected to be in the suspension regime, D_{susp}, as the largest grain for which $u_*/w_s \geq 1$ (Table DR3). Note that Cook et al. (2012) removed the constraint suppressing suspension-regime erosion in their implementation of the saltation-abrasion model such that they calculated non-zero erosion rates in reaches within the suspension regime. Viscous dampening of particle impacts is not expected to influence abrasion rates for floods which produced measurable erosion in the Da'an River due to the presence of coarse bed-material and large particle Stokes numbers.

DATA REPOSITORY FIGURE AND MOVIE CAPTIONS:

Figure DR1. (A) Mass erosion rate (E_m) and (B) volumetric erosion rate (E_v) for foam, rock, and concrete versus tensile strength (σ_T). Solid lines in (A) and (B) show power-law best fit to the data subject to the theoretical expectation that $E \propto \sigma_T^{-2}$ (Sklar and Dietrich, 2004). The similar scaling between erosion rate and tensile strength for variable-density foam and natural rock suggests that foam is a suitable rock analog. Circled triangles and dots correspond to the foam (σ_T = 0.32 MPa) and limestone (σ_T = 9.8 MPa) used in erosion-rate versus grain-size experiments (Figs. 3 and 4; Table DR1). Mass erosion rates from Sklar and Dietrich (2001) were converted to volumetric erosion rates using densities provided by L. Sklar (personal communication, 2014).

Figure DR2. Side view and bottom-up view photographs showing sediment transport for five different grain sizes in abrasion mill experiments. White arrows indicate flow direction. For both cases, an unerodible clear bed was used for easier visualization. For bottom-up view photographs, note the orientation of particle streaks (due to slow shutter speed) indicate transport dominantly in the azimuthal flow direction. The sediment free area at the center of the mill is the location where the propeller-induced vortex impinges on the bed. In side view photos, ruler on right shows units of cm; in bottom view photographs, the abrasion mill is 20 cm in diameter for scale. Grains of 2.0 and 2.4 mm diameter were intermediate between exclusive bed load and full suspension, moving via long hop lengths, but with hop height rarely exceeding the predicted maximum bedload layer height of ~1.5 cm using the Sklar and Dietrich (2004) empirical relationship.

Figure DR3. Erosion rate predicted with saltation-abrasion, total-load, and stream-power models under variable transport stage (τ_*/τ_{*c}) for conditions representative of the South Fork Eel River, California. Transport stage was varied by changing one of either grain size (D), flow depth (h), or slope (S), while (A) holding sediment supply (q_s) constant or (B) setting sediment supply to half of the transport capacity (q_{sc}). Note the saltation-abrasion model is dependent upon shear velocity, u_* (i.e., the product hS), rather than h or S individually. Following Sklar and Dietrich (2004) we set base values of D, h, S, and q_s to 60 cm, 0.95 m, 0.0053, and 8.9 x 10^{-4} m^2/s, respectively. For all models rock tensile strength was 7 MPa, Young's Modulus was 5 x 10^4 MPa, non-dimensional constant k_v was 10^6, and impacts with particle Stokes numbers < 75 were viscously damped. τ is bed shear stress.

Movie DR1. (MovieDR1.mp4) Side view of suspension-regime transport for D = 1.2 mm sand (u_*/w_s = 1.3) taken with a high speed camera (240 frame per second, total elapsed time is ~3.25 seconds).

Movie DR2. (MovieDR2.mp4)View looking up through clear abrasion mill with D = 1.2 mm sand in suspension-regime transport (u_*/w_s = 1.3) taken with a high speed camera (240 frame per second, total elapsed time is ~3.25 seconds). The abrasion mill is 20 cm in diameter.

Movie DR3. (MovieDR3.mp4)Side view of bedload regime transport for D = 6.8 mm gravel (u_*/w_s = 0.44) taken with a high speed camera (240 frame per second, total elapsed time is ~3.25 seconds).

Movie DR4. (MovieDR4.mp4)View looking up through clear abrasion mill of bedload regime transport for D = 6.8 mm gravel (u_*/w_s = 0.44) taken with a high speed camera (240 frame per second, total elapsed time is ~3.25 seconds). The abrasion mill is 20 cm in diameter. Note radial particle velocity due to secondary circulation exists, but is substantially smaller than azimuthal particle velocity.

DATA REPOSITORY REFERENCES

Beyeler, J.D., Sklar, L.S., Litwin, K., Johnson, J.P., Collins, G.C., and K.X. Whipple, 2009, The dependence of bedrock erodibility on rock material properties: Is tensile strength enough?: American Geophysical Union Fall Meeting, Abstract EP21C-0616, San Francisco, CA.

Cook, K. L., Turowski, J. M., and Hovius, N., 2012, A demonstration of the importance of bedload transport for fluvial bedrock erosion and knickpoint propagation: Earth Surface Processes and Landforms, v. 38, no. 7, p. 683-695, doi:doi: 10.1002/esp.3313.

Dietrich, W. E., 1982, Settling velocity of natural particles: Water Resources Research, v. 18, no. 6, p. 1615-1626, doi:10.1029/WR018i006p01615.

Dietrich, W. E., and Smith, J. D., 1983, Influence of the point-bar on flow through curved channels: Water Resources Research, v. 19, no. 5, p. 1173-1192, doi:10.1029/WR019i005p01173.

Engle, P., 1978, Impact wear of materials: New York, Elsevier Science.

Fernandez-Luque, R., and R. van Beek, 1976, Erosion and transport of bedload sediment: Journal of Hydrualic Research, v. 14, p. 127-144, doi:10.1080/00221687609499677.

Howard, A. D., and Kerby, G., 1983, Channel changes in badlands: Geological Society of America Bulletin, v. 94, no. 6, p. 739-752.

Lamb, M. P., Dietrich, W. E., and Sklar, L. S., 2008, A model for fluvial bedrock incision by impacting suspended and bed load sediment: Journal of Geophysical Research-Earth Surface, v. 113, no. F3, doi:10.1029/2007jf000915.

Leopold, L. B., Wolman, M. G., and Miller, J. P., 1964, Fluvial processes in geomorphology, San Francisco, W.H. Freeman and Company.

McLean, S. R., 1992, On the calculation of suspended-load for noncohesive sediments: Journal of Geophysical Research-Oceans, v. 97, no. C4, p. 5759-5770, doi:10.1029/91jc02933.

Nikora, V., and Roy, A. G., 2012, Secondary flows in rivers: Theoretical framework, recent advances, and current challenges, *in* Church, M., Biron, P. M., and Roy, A. G., eds., Gravel-bed rivers: Processes, tools, environments, John Wiley & Sons, West Sussex, United Kingdom, p. 3-22.

Rouse, H. R., 1937, Modern conceptions of the mechanics of turbulence: Trans. Am. Soc. Civ. Eng., v. 102, no. 1, p. 463-543,

Sklar, L. S., and Dietrich, W. E., 2001, Sediment and rock strength controls on river incision into bedrock: Geology, v. 29, no. 12, p. 1087-1090, doi:10.1130/0091-7613(2001)029<1087:sarsco>2.0.co;2.

Sklar, L. S., and Dietrich, W. E., 2004, A mechanistic model for river incision into bedrock by saltating bed load: Water Resources Research, v. 40, no. 6, doi:10.1029/2003wr002496.

Sklar, L. S., and Dietrich, W. E., 2006, The role of sediment in controlling steady-state bedrock channel slope: Implications of the saltation-abrasion incision model: Geomorphology, v. 82, no. 1-2, p. 58-83, doi:10.1016/j.geomorph.2005.08.019.

Sklar, L. S., and Dietrich, W. E., 2008, Implications of the saltation-abrasion bedrock incision model for steady-state river longitudinal profile relief and concavity: Earth Surface Processes and Landforms, v. 33, no. 7, p. 1129-1151, doi:10.1002/esp.1689.

Winterstein, T., and Stefan, H., 1983, Suspended sediment sampling in flowing water: Laboratory study of the effects of nozzle orientation withdrawal rate and particle size: Saint Anthony Falls Laboratory, External Memorandum M-168, University of Minnesota, 97 p.

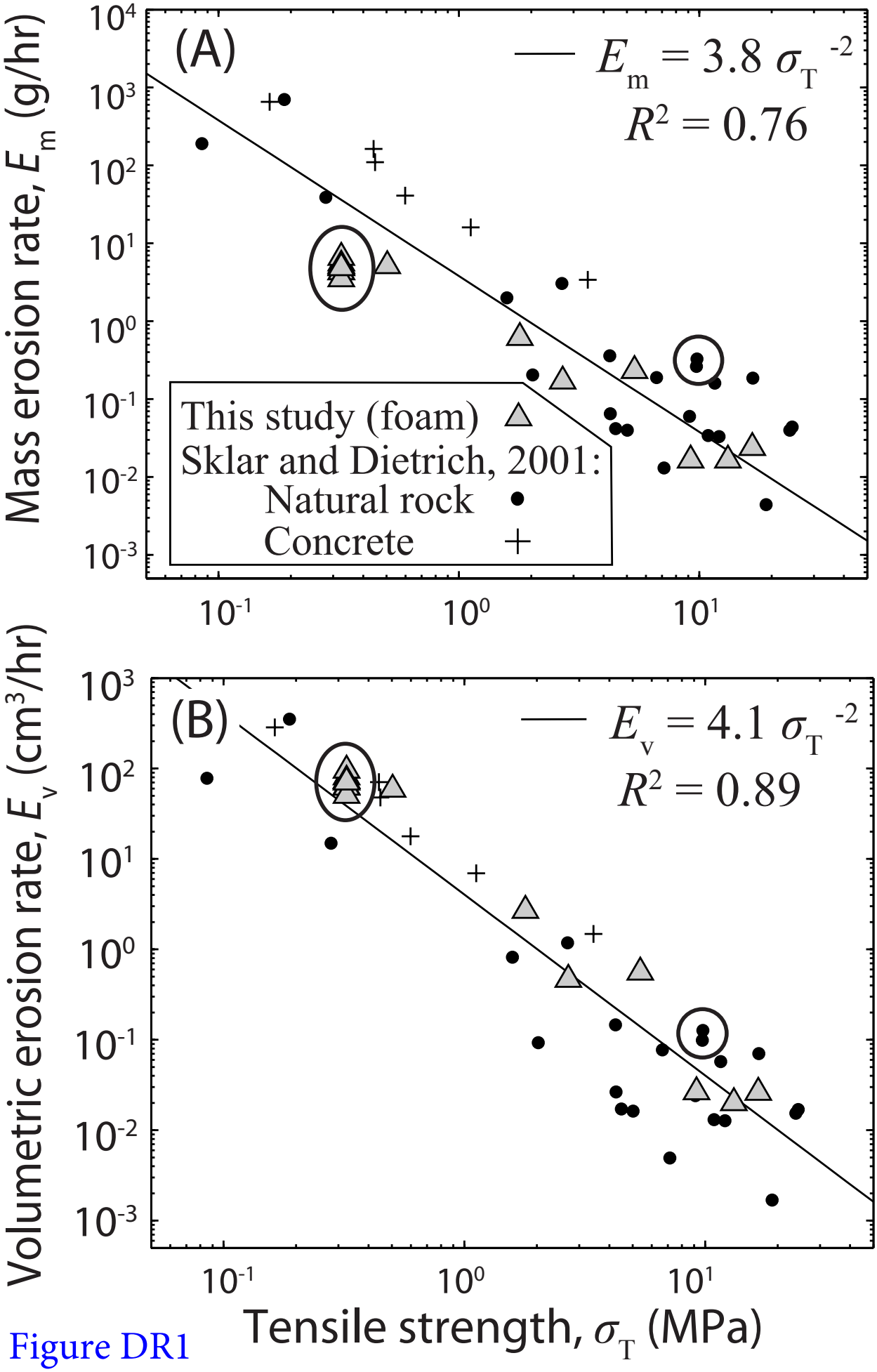
(A)
$E_m = 3.8\ \sigma_T^{-2}$
$R^2 = 0.76$
This study (foam)
Sklar and Dietrich, 2001:
Natural rock
Concrete
Mass erosion rate, E_m (g/hr)
(B)
$E_v = 4.1\ \sigma_T^{-2}$
$R^2 = 0.89$
Volumetric erosion rate, E_v (cm^3/hr)
Tensile strength, σ_T (MPa)

Figure DR1

Figure DR2

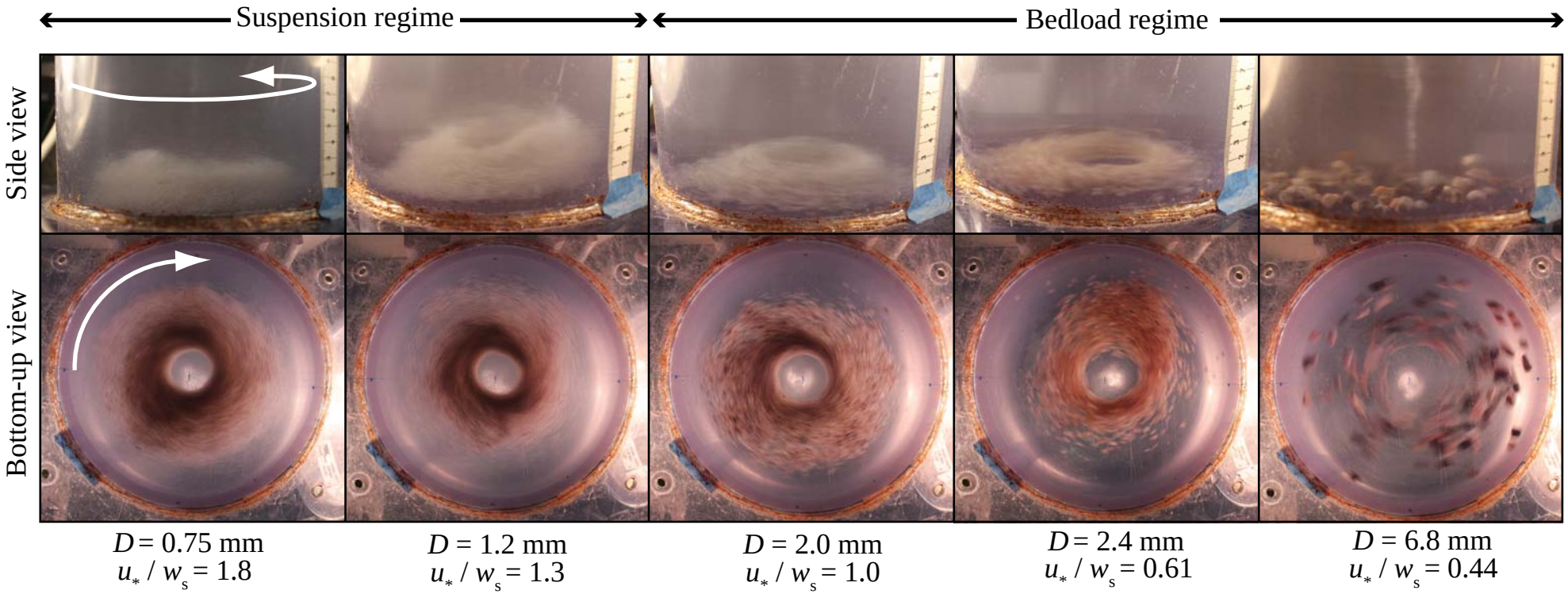
Suspension regime
Bedload regime
Side view
Bottom-up view
D = 0.75 mm
u* / ws = 1.8
D = 1.2 mm
u* / ws = 1.3
D = 2.0 mm
u* / ws = 1.0
D = 2.4 mm
u* / ws = 0.61
D = 6.8 mm
u* / ws = 0.44

Figure DR3

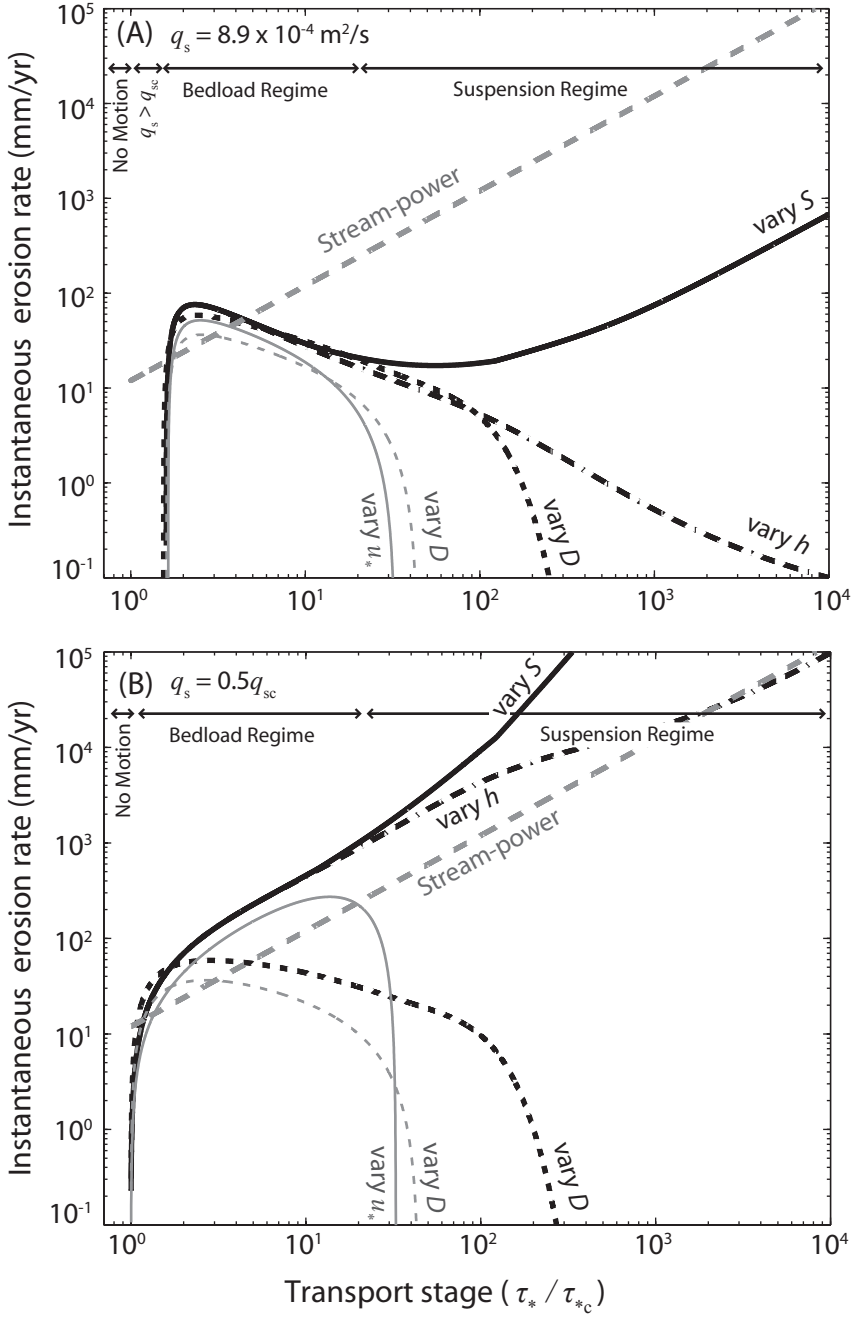

Total-load (Lamb et al., 2008):

- h = 0.95 m, D = 60 mm, variable S
- S = 0.0053, D = 60 mm, variable h
- S = 0.0053, h = 0.95 m, variable D

Saltation-abrasion (Sklar and Dietrich, 2004):

- D = 60 mm, variable u_*
- u_* = 0.22 m/s, variable D

Stream-power:

- $E = 0.41(\tau^1)$

Table DR1: Erosion rates for sediment of varying grain size under constant sediment load and shear stress*

Experiment ID	D_{16} (mm)	D (mm)	D_{84} (mm)	Volume Eroded (cm^3)	Measurement Technique†	Time Eroded (hr)	Volumetric Erosion Rate (cm^3/hr)	u_*/w_s §	% Viscously-Damped Impacts#	Corey Shape Factor	Powers Roundness
D-0.46-A	0.34	0.46	0.58	4.9	Scan	365.4	0.0134	2.9	99.7	0.5	2.5
D-0.46-B	0.34	0.46	0.58	6.1	Scan	365.4	0.0167	2.9	99.7	0.5	2.5
D-0.46-C	0.34	0.46	0.58	4.5	Scan	365.4	0.0122	2.9	99.7	0.5	2.5
D-0.46-D	0.34	0.46	0.58	6.6	Scan	430.0	0.0153	2.9	99.7	0.5	2.5
D-0.46-E	0.34	0.46	0.58	3.2	Scan	430.0	0.00746	2.9	99.7	0.5	2.5
D-0.46-F	0.34	0.46	0.58	4.9	Scan	430.0	0.0113	2.9	99.7	0.5	2.5
D-0.75-A	0.56	0.75	0.99	6.2	Scan	21.0	0.295	1.8	82.3	0.5	2.5
D-0.75-B	0.56	0.75	0.99	5.5	Scan	21.0	0.261	1.8	82.3	0.5	2.5
D-0.75-C	0.56	0.75	0.99	8.7	Scan	21.0	0.413	1.8	82.3	0.5	2.5
D-1.2-A	0.89	1.20	1.58	9.7	Scan	5.0	1.94	1.3	35.5	0.5	2.5
D-1.2-B	0.89	1.20	1.58	12.2	Scan	5.0	2.44	1.3	35.5	0.5	2.5
D-1.2-C	0.89	1.20	1.58	9.9	Scan	5.0	1.97	1.3	35.5	0.5	2.5
D-1.2-D	0.89	1.20	1.58	6.1	Scan	2.5	2.45	1.3	35.5	0.5	2.5
D-2.0-A	1.55	2.02	2.50	25.5	Scan	1.5	17.0	1.00	7.26	0.48	2.5
D-2.0-B	1.55	2.02	2.50	29.8	Scan	1.5	19.8	1.00	7.26	0.48	2.5
D-2.0-C	1.55	2.02	2.50	29.8	Scan	1.5	19.9	1.00	7.26	0.48	2.5
D-2.0-D	1.55	2.02	2.50	23.5	Scan	1.5	15.6	1.00	7.26	0.48	2.5
D-2.4-A	2.0	2.4	2.8	73.0	Scan	1.5	48.6	0.61	3.77	0.69	5
D-2.4-A	2.0	2.4	2.8	60.0	Scan	1.5	40.0	0.61	3.77	0.69	5
D-6.8-A	5.6	6.8	8.0	29.8	Scan	0.3	89.3	0.44	<0.1	0.57	3.5
D-6.8-A	5.6	6.8	8.0	29.8	Scan	0.3	89.3	0.44	<0.1	0.57	3.5
D-6.8-A	5.6	6.8	8.0	58.0	Scan	0.3	174	0.44	<0.1	0.57	3.5
D-24-A	22.0	24.0	26.0	292.2	Scale	1.0	292	0.25	<0.01	0.5	4.5
D-24-B	22.0	24.0	26.0	156.3	Scale	0.5	313	0.25	<0.01	0.5	4.5
D-24-C	22.0	24.0	26.0	73.4	Scale	0.4	176	0.25	<0.01	0.5	4.5
D-24-D	22.0	24.0	26.0	40.6	Scale	0.4	97.5	0.25	<0.01	0.5	4.5
D-24-E	22.0	24.0	26.0	39.1	Scale	0.4	93.8	0.25	<0.01	0.5	4.5
D-40-A	-	40.9	-	182.8	Scale	0.5	366	0.16	<0.01	0.65	5.5
D-40-B	-	43.7	-	121.9	Scale	0.5	244	0.15	<0.01	0.65	5.5

[*] For all experiments, sediment loading was 70 g, propeller was set to 1000 RPM, and the substrate was 0.064 g/cm^3 foam with 0.324 MPa tensile strength and 3.92 MPa Young's modulus. Grains 2.02 mm in diameter and smaller were measured via particle image analysis with a Microtrac DIA, and D_{16}, D, and D_{84} are the 16th percentile, median, and 84th percentile grain size of the sediment used for erosion. Grains 2.4 mm in diameter and larger were hand sieved and manually measured; for these grains, D_{16}, D, and D_{84} represent the lower limit, average, and upper limit of the particle distribution, respectively. A single grain was used where D_{16} and D_{84} are not reported.

[†] Scan refers to eroded volume measured with sub-mm precision laser scanning, and scale refers to mass eroded measured with 0.1-g precision dry-weighing before and after experiments. The two methods gave similar results when both were performed, for certain cases mass loss measurements were advantageous over volume loss measurements, and vice versa (for example, low-density foam with small erooded volumes leads to negligible mass loss such that scan measurements are more accurate).

[§] u_* is the fluid shear velocity. w_s is the terminal settling velocity calculated for particles of size D using measured values of Corey Shape Factor and Powers Roundess and the Dietrich (1982) empirical formula.

[#] Percent of viscously damped impacts was calculated for particles of size D assuming damping of impacts for Stokes numbers <75, and impact velocities based on particle fall height and Gaussian turbulent fluctuations as parametrized in Lamb et al (2008).

Table DR2: Erosion rate for foam of varying tensile strength and Young's modulus*

Experiment ID	Tensile Strength (MPa)	Young's Modulus (MPa)	Density (g/cm^3)	Run Time (hr)	Mass Loss (g)	Volumetric Erosion Rate (cm^3/hr)
Tensile-1-A	0.32	3.92	0.064	1.0	5.6	87.4
Tensile-1-B	0.32	3.92	0.064	1.0	6.6	103
Tensile-1-C	0.32	3.92	0.064	1.0	4.3	67.1
Tensile-1-D	0.32	3.92	0.064	1.0	5.2	81.2
Tensile-1-E	0.32	3.92	0.064	1.0	4.3	67.1
Tensile-1-F	0.32	3.92	0.064	2.0	7.0	54.6
Tensile-1-G	0.32	3.92	0.064	2.0	10.0	78.0
Tensile-1-H	0.32	3.92	0.064	2.0	9.7	75.7
Tensile-1-I	0.32	3.92	0.064	0.7	21.0	447
Tensile-2	0.50	5.38	0.096	4.0	20.6	53.6
Tensile-3	1.79	25.58	0.240	18.0	11.1	2.57
Tensile-4	2.70	47.18	0.320	67.0	11.4	0.531
Tensile-5	5.38	104.80	0.481	71.4	16.6	0.484
Tensile-6	9.20	186.04	0.641	121.2	2.0	0.026
Tensile-7	13.17	265.79	0.769	121.2	2.0	0.021
Tensile-8	16.62	329.56	0.961	168.0	4.0	0.025

* For all experiments, sediment loading was 150 g of 5.6-6.3 mm sieved grains, and propeller was set to 1000 RPM. Mass loss measurements were made by weighing discs before and after the experiment with a 0.1-g precision scale. Eroded discs are commercially available closed cell polyurethane foam (http://precisionboard.com). Tensile strength and Young's modulus are measured by the manufacturer using standard procedures (American Society for Testing and Materials standard D-1623).

Table DR3: Da'an River suspension calculations[*]

Reach	Shields Stress	Bed Shear Stress (Pa)	D_{susp} [†] (cm)	Transport Stage[§]
Pre-uplift/upstream of uplift	0.091	221	0.98	2.0
Pond in 1999	0.016	38.8	0.19	0.36
Upstream of hinge	0.081	197	0.86	1.8
Downstream of hinge	0.18	437	2.2	4.0
Scarp/knickpoint in 2001	1.02	2480	15	23
Pond in 2004	0.047	114	0.50	1.0
Narrow knickpoint	50.6	123000	110	1100
Knickzone	0.4	971	6.1	8.9
Gorge downstream of knickzone in 2010	0.11	267	1.2	2.4

[*] Shields stress data and reach naming convention as reported by Cook et al. (2012). All calculations based on a water discharge of 1300 m^3/s.

[†] D_{susp} is the largest grain size capable of being within the suspension regime for the reported bed shear stress.

[§] Transport stage calculated assuming a critical Shields Stress of 0.045 (Cook et al., 2012).